Journal of Power Sources 282 (2015) 34–44

Contents lists available at ScienceDirect

Journal of Power Sources

journal homepage: www.elsevier.com/locate/jpowsour

On the design of Pt based catalysts. Combining porous architecture with surface modification by Sn for electrocatalytic activity enhancement

Jonathan Flórez-Montaño [a], Gonzalo García [a], José L. Rodríguez [a], Elena Pastor [a, *], Paula Cappellari [b], Gabriel A. Planes [b]

[a] Instituto Universitario de Materiales y Nanotecnología, Universidad de La Laguna, Astrofísico F. Sánchez s/n, 38071 La Laguna, Tenerife, Spain
[b] Departamento de Química, Universidad Nacional de Río Cuarto, Agencia Postal 3, 5800 Río Cuarto, Argentina

HIGHLIGHTS

- Mesoporous Pt material (MPPt) was successfully modified by Sn adatoms (MPPt/Sn).
- The CO tolerance was evaluated at MPPt, MPPt/Sn and commercial Pt_3Sn/C catalysts.
- The catalytic activity toward methanol oxidation for all electrodes was evaluated.
- CO and methanol oxidation reactions were studied at 25 and 60 °C by DEMS.
- Energy conversion efficiency from methanol to CO_2 for all catalysts was calculated.

GRAPHICAL ABSTRACT

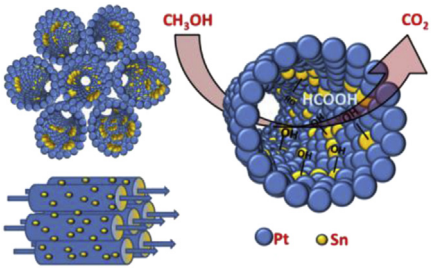

ARTICLE INFO

Article history:
Received 16 October 2014
Received in revised form
2 January 2015
Accepted 4 February 2015
Available online 7 February 2015

Keywords:
DMFC
DEMS
Mesoporous electrodes
CO oxidation
Methanol oxidation
Pt-based materials

ABSTRACT

Metallic mesoporous (MP) catalysts with large surface area can be obtained *in-situ*, in a single step, by electrochemical reduction. In this work, the electrochemical behavior of MPPt and Sn modified mesoporous Pt (MPPt/Sn) was studied and compared with commercial carbon supported PtSn alloy (3:1). The electrochemical activity toward carbon monoxide and methanol oxidation reactions were evaluated by cyclic voltammetry and chronoamperometry, whereas X-ray photoelectron spectroscopy was used to determine the surface composition and oxidation state of the atoms in the top layers of the catalysts. The analysis of methanol conversion to CO_2 was performed with aid of differential electrochemical mass spectrometry (DEMS). Results reveal a better performance of the MPPt/Sn, which shows higher current density and energy conversion efficiency of fuel to CO_2 than conventional carbon supported PtSn alloy (3:1).

1. Introduction

Direct methanol fuel cells (DMFC) are devices that produce energy from an electrochemical reaction. Main differences

* Corresponding author.
E-mail address: epastor@ull.edu.es (E. Pastor).

http://dx.doi.org/10.1016/j.jpowsour.2015.02.018
0378-7753/

between DMFC and conventional batteries are the use of a liquid combustible, continuous operating capability and high thermodynamic efficiency limit [1]. Thus, DMFC have been proposed as suitable power devices for mobile applications. All the advantages mentioned before, allows envisage the DMFC technology like a suitable transition to a completely clean energy generation [2–4].

Conversely, some serious weaknesses delay the commercial utilization of DMFC. One of the most important difficulties is the cost of the novel metal required for the electrocatalytic process used at both electrodes (mainly Pt and some of its alloys) [5–8]. Also kinetic restrictions must be overcome for a better metal utilization at the cathode (oxygen reduction reaction, ORR) [9–11], Additionally, a better performance of the anode becomes necessary. With these purposes, the use of lower noble metal loading with high surface accessibility and low poisoning of the active sites by reaction intermediates (i.e. CO, HCHO, HCOOH) is required [12].

The economic problem associated to the catalysts production is an important reason, but not the only one, for build-up nanostructured electrodes. Since electrochemical processes are almost of superficial nature, the fabrication of nanostructured catalysts presents the most powerful approach for the production of small electrodes with high surface area and low metal loading [13,14]. However, this approach introduces some intrinsic difficulties like metallic surface stability in the nanometer scale, and mass transport requirements for reactants and products [15].

There are different ways to prepare practical catalysts for DMFC [16,17]. Generally catalysts utilized as electrodes in PEM fuel cells comprise noble metal nanoparticles supported on high surface carbon (e.g. Pt/C, Pt–Ru/C, etc.). The most widespread route to synthesize this kind of catalysts involves the chemical reduction of the precious metal after its impregnation onto the catalyst support [16–21]. While various synthetic approaches were intended, the design of well-defined mesoporous catalysts persist as one of the most promising objectives [16].

During the last decade, some publications have focused on the study of unsupported electrodes (e.g. mesoporous metal catalysts) [22–25]. In this context, metallic mesoporous (MP) catalysts are interesting because they can be obtained *in-situ* by chemical or electrochemical reduction of the metal cations present in the aqueous phase of a liquid crystalline solution. Usually, this single process renders thin electrodes with high surface area, with the additional advantage that their architecture can be easily tuned by adjusting of the synthesis parameters (i.e. the porous radio can be adjusted by the choice of the appropriated surfactant, and additional porosity can be introduced by the selection of the applied potential). The resulting catalysts possess an extremely concave mesoporous surface, and this characteristic may, by itself, affect the CO electrooxidation reaction [26].

On the other hand, the search for more active surfaces has led to surface modification by adatoms (Pt/M) of diverse nature. Consequently, the Pt surface has been broadly modified by spontaneous deposition of metal [23,26–28]. This approach is even more interesting when combined with mesoporous Pt surface.

For this reasons, in the present work MPPt surfaces were modified by Sn adatoms (MPPt/Sn) and employed in order to understand the effect of mesoporous surface modification by oxophilic atoms toward the methanol electrooxidation reaction. Consequently, the electrochemical properties of the synthesized MPPt/Sn electrodes were examined by the CO and methanol oxidation reactions and compared with a commercial catalyst (Pt_3Sn/C, E-TEK). In addition, *in situ* differential electrochemical mass spectroscopy (DEMS) measurements were carried out with the aim to quantify the CH_3OH conversion to CO_2.

2. Experimental

2.1. Physicochemical characterization

The XPS characterization of the samples was performed in a UHV chamber (base pressure $< 5 \times 10^{-9}$mbar), equipped with a double anode X-ray source (Omicron) and a hemispherical electronanalyzer (VG Scienta). All XPS measurements were performed at room temperature, using non-monochromatic Mg–K radiation (h = 1253.6 eV) and a pass energy of 50 eV and 20 eV for the survey and high-resolution spectra, respectively.

2.2. Electrochemical measurements

A thermostatized three electrodes electrochemical cell was used to realize the analysis at 25 and 60 °C. This electrochemical cell allows solution exchange holding the potential control on the working electrode. For the study of CO tolerance a 0.5 M H_2SO_4 solution was used, while that for the methanol oxidation reaction a 0.5 M H_2SO_4 + 0.1 M CH_3OH solution was utilized at both temperatures. The cell includes a carbon as counter electrode and a reference hydrogen electrode (RHE) in the electrolyte. All potentials in this work are given against the RHE. Electrochemical measurements were performed with a PC Autolab potentiostat-galvanostat. All reagents were analytical grade. Argon (N50) was bubbled through the solution to avoid dissolved oxygen. CO (N47) was employed for the adsorption experiences. In this work, currents are expressed as current densities J (A cm^{-2}), calculated from the measured current I (A) and the real electroactive area S. The electroactive area S was estimated from the CO stripping experiences. With this purpose, CO was bubbled for 10 min at 0.2 V vs. RHE and subsequently argon for 30 min was used to degas the solution during 30 min. After that, the potential was scanned from the adsorption potential down to 0.05 V (so the hydrogen adsorption region can be checked) and then up to 0.90 V, and three consecutive cycles were recorded at 0.005 V s^{-1}. First cycle corresponds to the CO_{ads} electrooxidation, while the second and third cycles show the background voltammogram, indicating that all adsorbed carbon monoxide was completely removed from the catalyst surface.

2.3. DEMS setup

The gaseous species produced on the electro-active surface can be followed on-line by mass spectrometry. For detection of the ion current during mass spectrometric measurement, Quadstar™ 422-software (Pfeiffer-vacumm Thermostar) was used. The setup allows the detection of the ion current for each m/z separately. A conventional electrochemical cell was used and the meniscus configuration was adopted. The working electrode surface is placed very close (~micrometers) to a Teflon capillary, which is connected directly to the vacuum of the mass spectrometer. Details of the setup can be found elsewhere [29].

2.4. DEMS calibration

The calculation of the efficiency for methanol conversion to CO_2 by DEMS requires a previous determination of the $m/z = 44$ calibration constant (K^{CO_2}). This constant correlates the number of CO_2 molecules generated on the electrode surface (through the faradaic charge) with the portion of this molecules captured by the mass spectrometer (proportional to $m/z = 44$ ion current). K^{CO_2} has to be determined before each experiment because it depends of several variables (membrane-electrode gap, flow rate, temperature and pressure in the mass vacuum line). The calibration constant is calculated as follow: faradaic ($Q_f^{CO_2}$) and ionic $m/z = 44$ ($Q_i^{CO_2}$)

charges were calculated from CO stripping and related according to equation:

$$K^{CO_2} = 2\frac{Q_i^{CO_2}}{Q_f^{CO_2}} \quad (1)$$

Then, the current efficiency E for methanol electrooxidation to CO_2 is determined from the subsequent equation:

$$E^{CO_2} = \frac{6*Q_i^{CO_2}}{K^{CO_2}*Q_f^T} \quad (2)$$

where Q_f^T is the charge associated to all faradaic processes at the surface.

Cyclic voltammograms (CVs) and mass spectrometry cyclic voltammograms (MSCVs) for CO_{ads} and methanol at MP electrodes in sulphuric acid were recorded at 5 and 2 mV s^{-1}. Current transients (CTs) and mass spectrometry current transients (MSCTs) for methanol oxidation at MP electrodes in sulphuric acid were recorded at 0.55 and 0.65 V.

2.5. Working electrode preparation

Mesoporous Pt electrodes were obtained by electrochemical reduction of a mixture of aqueous hexachloroplatinic acid (8%) and octaethylene glycol monohexadecyl ether ($C_{16}EO_8$) (50% weight fraction) onto a DEMS Au disk electrode (Ø = 1 mm) at 60 °C and 0.15 V. Typically, after 10 min of Pt^{+4} reduction a charge of 724 mC cm^{-2} was deposited onto Au substrate, resulting in a mesoporous Pt layer containing 1.94×10^{-4} g of Pt (assuming 75% efficiency). Then, the electrode was leaved in distilled water for 48 h, to let the surfactant be completely removed from the porous structure. The surface modification by Sn adatoms was obtained in the following way: an MP Pt electrode was immersed in 0.5 mM $SnSO_4$/0.5 M H_2SO_4 fresh solution for 5 min. This last step facilities the Sn dispersion inside the porous structure. After that, the electrode was rinsed with water, and finally transferred to an electrochemical cell containing 0.5 M H_2SO_4. Finally, the electrode was cycled between 0.05 and 0.50 V to reduce the adsorbed Sn precursor to metallic Sn. The last procedure was repeated as many times necessary.

For studies of the carbon-supported Pt_3Sn/C E-TEK catalyst, the working electrode consists of a certain amount of the Pt_3Sn/C powder (20 wt. % metal supported on Vulcan XC-72, ETEK) deposited as a thin layer over a glassy carbon disc (Ø = 7 mm). For this purpose, an aqueous suspension of 1.0 mg mL^{-1} of the Pt_3Sn/C catalyst was prepared by ultrasonic dispersion of 2.0 mg of the Pt_3Sn/C catalyst in 15 μL of Nafion (5 wt. % Aldrich) and pure water (0.5 mL). An aliquot (10 μL) of the dispersed suspension was pipetted on a glassy carbon surface (7 mm diameter) and dried at ambient temperature under Ar atmosphere.

3. Results and discussion

3.1. MPPt catalyst modified by Sn adatoms

Fig. 1 shows the variation of the hydrogen adsorption/desorption area and the Sn coverage degree for different Sn adsorption times (in several exposition steps, the time is expressed accumulatively). Each step involves the introduction of the MPPt working electrode into a Sn solution for 5 min and a subsequent electrochemical reduction. The degree of Sn coverage was calculated using the following equation [30–34].

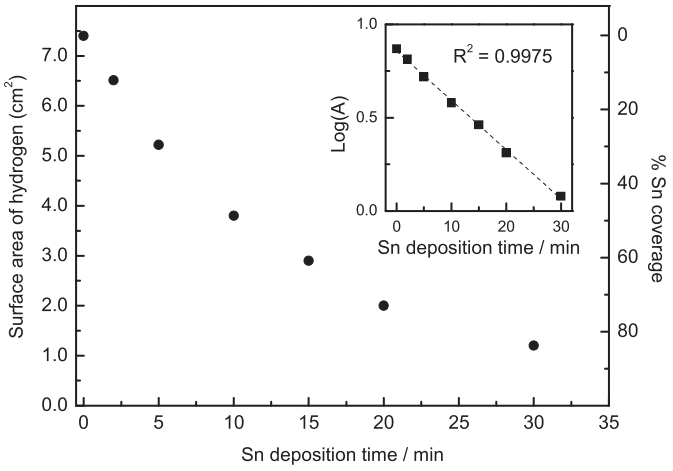

Fig. 1. Pt surface area calculated from the hydrogen adsorption/desorption region (left Y-axis), and Sn coverage percentage at different adsorption times (right Y-axis) vs adsorption time. Inset: Logarithmic behavior of the deposition current.

$$\theta_{Sn} = \frac{Q_H^b - Q_H^a}{Q_H^b} \quad (3)$$

Q_H^a is the electrical charge for the MPPt/Sn, evaluated from cyclic voltammetry in the potential region between 0.05 and 0.40 V_{HRE}, and Q_H^b is the electric charge for the MPPt at the same potential region. A close inspection of Fig. 1 reveals that the most significant change in the Sn coverage occurs between 5 and 15 min. The inset graph shows that the Sn deposition process follows an exponential behavior. The slope points out that, for each Sn deposition step, the available (Sn-free) Pt surface is reduced about 20%. Additionally, no substantial increment in the charge is observed for longer Sn deposition time, indicating that the process operates self-poisoning the Pt surface, as was early reported by Gupta et al. [35]. Considering that in the present case only a small change occurs for more than three deposition steps, the study is limited to 15 min that corresponds to $\theta_{Sn} = 0.60$. In this sense, it was reported high activity towards methanol oxidation with similar nominal value of Sn modified Pt catalysts in acidic media [36].

The cyclic voltammograms for MPPt and MPPt/Sn electrodes in sulphuric acid solution are given in Fig. 2. The black line corresponds to the current response for the unmodified MPPt material, in which is well visible the hydrogen adsorption/desorption (H_a/H_d) region between 0.05 and 0.4 V. At potentials above 0.4 V, a non-faradaic process is observed along the double layer region (between 0.4 and 0.8 V). Finally, the slight increment of the anodic current at E > 0.8 V indicates the formation of oxygenated species onto the Pt surface, i.e. the onset potential for Pt oxides formation. The effect of the Sn adatoms on the MPPt surface (red, green and blue lines) is noticeable by the charge fall in the H_a/H_d region, especially in the sites related with (100) and (110) surface orientations [37]. Additionally, it is observed a new contribution at ca. 0.73 V, corresponding to the onset for the Sn oxidation process. Also, it can be discerned that as the Sn coverage rises with the successive exposition steps, the Sn oxide redox couple around 0.75 and 0.62 V is notoriously increased. As was described above, the surface blocking effect by Sn adatoms in the H_a/H_d region will be used later to estimate the Sn coverage (θ_{Sn}) [34,35].

All these results are consistent with those reported previously by other authors for PtSn alloys [19], carbon supported PtSn nanoparticles [20] and Pt single crystal structures modified by Sn [21,34]. The double layer broadening has usually been attributed to

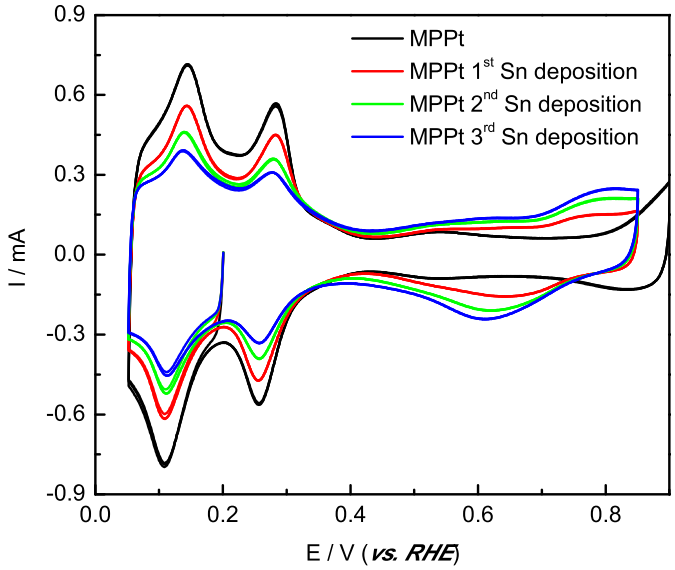

Fig. 2. Cyclic voltammograms obtained for MPPt and MPPt/Sn catalysts in 0.5 M H_2SO_4 solution at a scan rate of 100 mV s^{-1} and 25 °C.

H_2O activation on Sn and/or SnO_2 species, while the anodic peak around 0.7 V is associated to Sn oxide (SnO_2) formation from the dissociation of H_2O on the metallic surface [30–32,35].

The application of techniques as Energy Dispersive X-Ray Spectroscopy (EDX) or X-Ray Diffraction (XRD) for the detection of Sn in the sample is not possible as the amount of Sn is very small (the surface is covered only by ad-atoms of Sn) and it is not present in a crystalline form. For this reason, the surface constituent phase of the MPPt and MPPt/Sn (θ_{Sn} = 0.60) materials were further studied by XPS analysis which is more appropriated as a surface sensitive technique. Fig. 3A displays the Pt 4f XPS spectra that contain two peaks corresponding to the Pt $4f_{7/2}$ and Pt $4f_{5/2}$ states. Each peak was deconvoluted and associated to three different Pt oxidation states (Pt^0, Pt^{2+} and a small contribution of Pt^{4+}).

MPPt develops a $4f_{7/2}$ signal that can be correlated to three curves peaked at 71.0, 72.1 and 73.3 eV, which are attributed to Pt^0, Pt^{2+} (PtO and $Pt(OH)_2$-like species) and Pt^{4+}, respectively [39,40]. On the other hand, MPPt/Sn spectra (Fig. 3B) shows similar signals than MPPt, but at small shift of B.E. toward higher values can be discerned, i.e. Pt^0, Pt^{2+} and Pt^{4+} curves appear centered at 71.0, 72.5 and 73.8 eV, respectively. However, the most important finding is the change in their relative area that is associated to the amount of the species in the catalyst surface (Table 1). The Sn 3d signal of the MPPt/Sn was also deconvoluted into two distinguishable doublets (Fig. 3C) with different intensities. In this context, the $3d_{5/2}$ peaks at 484.6 and 486.5 eV are attributed to metallic Sn^0 and SnO_2 species [30,40].

Table 1 shows that MPt/Sn catalyst surface is almost composed by Sn and Pt species in the oxide (SnO_2) and metallic (Pt^0) states, respectively. The last is caused by electronegativity differences between Pt and Sn, leading to a charge transfer from the less electronegative Sn to the more electronegative Pt.

Furthermore, the spectra developed by the modified material after three Sn deposition steps reveals a surface atomic ratio of Pt:Sn of 40:60, which is in total agreement with the calculated by the charge decrease in the hydrogen adsorption/desorption potential region. In this context, it is important to remind that both XPS and cyclic voltammetry are surface sensitive techniques, and this is the reason for the excellent correlation.

Therefore, it can be extracted from these results that the catalyst surface is mainly formed by metallic Pt and SnO_2 located mainly on Pt sites with (110) and (100) orientations, in addition to rather similar mass percent composition of both elements [40].

3.2. CO stripping

The oxidative desorption of a CO monolayer adsorbed on a catalyst surface (denoted here as CO stripping) is an important tool for surface characterization. Since adsorbed CO is a strong catalyst poison and it is a reaction intermediate during, for example, the methanol and formic acid electrooxidation reaction, its removal is a key factor to be investigated [23,24]. Furthermore, the CO stripping is a powerful technique for the study of the surface morphology and structure. In addition, CO stripping is a convenient method to obtain an accurate estimation of the electroactive surface area [26,41].

The left side of Fig. 4 (panels denoted as A, C and E) shows CO stripping experiments for MPPt, MPPt/Sn (θ_{Sn} = 0.60) and commercial Pt_3Sn/C E-TEK electrodes recorded at two different temperatures (25 and 60 °C) in 0.5 M H_2SO_4 at 5 mV s^{-1}. It is observed that for all catalysts the onset and peak potentials for CO oxidation reaction shift toward more negative values with the increment of the temperature. However, some differences between them can be found. MPPt material develops an onset potential at ca. 0.45 V_{RHE} and a smooth anodic wave (or pre-peak) centered at ca. 0.55 V_{RHE} that is followed by a sharp anodic peak at 0.7 V_{RHE} at 25 °C. The rise of the temperature shifts all these features about 0.1 V towards more negative potentials.

In contrast, MPPt/Sn catalyst with θ_{Sn} = 0.60 presents the onset potential for the CO stripping at much lower values (0.23 V_{RHE}) than MPPt at 25 °C. Additionally, the CO stripping profile recorded at 25 °C for MPPt/Sn electrode develops two well-defined anodic peaks centered at ca. 0.4 (denoted as I) and 0.67 V_{RHE} (denoted as II). These results are consistent with those reported by other authors in the literature [30–36,38], in which a Sn promoter effect was observed. In fact, Sn is capable to promote the oxidation of adsorbed CO [42,43] with the aid of adsorbed oxygenated species (i.e. OH species), which are produced at lower potentials than Pt. The increasing of the temperature to 60 °C does not shift the onset and peak potential developed at 0.4 V (I) but increases the faradaic charge in this potential region. Additionally, it is observed a current charge diminution and a shift to lower potentials of the second anodic peak (II) with the rise of the temperature. These results indicate the existence of sites with different catalytic activity towards the CO oxidation reaction at MPPt/Sn, and suggest a CO surface diffusion from the least (II) to the most (I) active sites, which increases with the temperature [44].

On the other hand, CO_{ad} oxidation on commercial Pt_3Sn/C electrode shows a broad anodic peak with an onset and peak potential at ca. 0.25 and 0.75 V, respectively. It is noticeable the higher value of the CO peak potential developed by the commercial Pt_3Sn/C catalyst in comparison with the MPPt and MPPt/Sn materials. Similar to the observed for both MP electrodes, the CO peak potential for the Pt_3Sn/C shifts negatively with the increment of the temperature.

Results are consistent with an enhancement of the water activation process (adsorbed oxygenated species formation) due to the introduction of Sn and the rise of the temperature, which affect the CO electrooxidation by means of the bi-functional mechanism [31–36,42]. Nevertheless, small contribution from electronic effect cannot be discarded.

The recorded mass spectrometric cyclic voltammograms (MSCVs) related to CO_2 formation (m/z = 44) for each material are given at the right side of Fig. 4 (panels denoted as B, D and F). This figure clearly shows a close correlation between faradaic and ionic

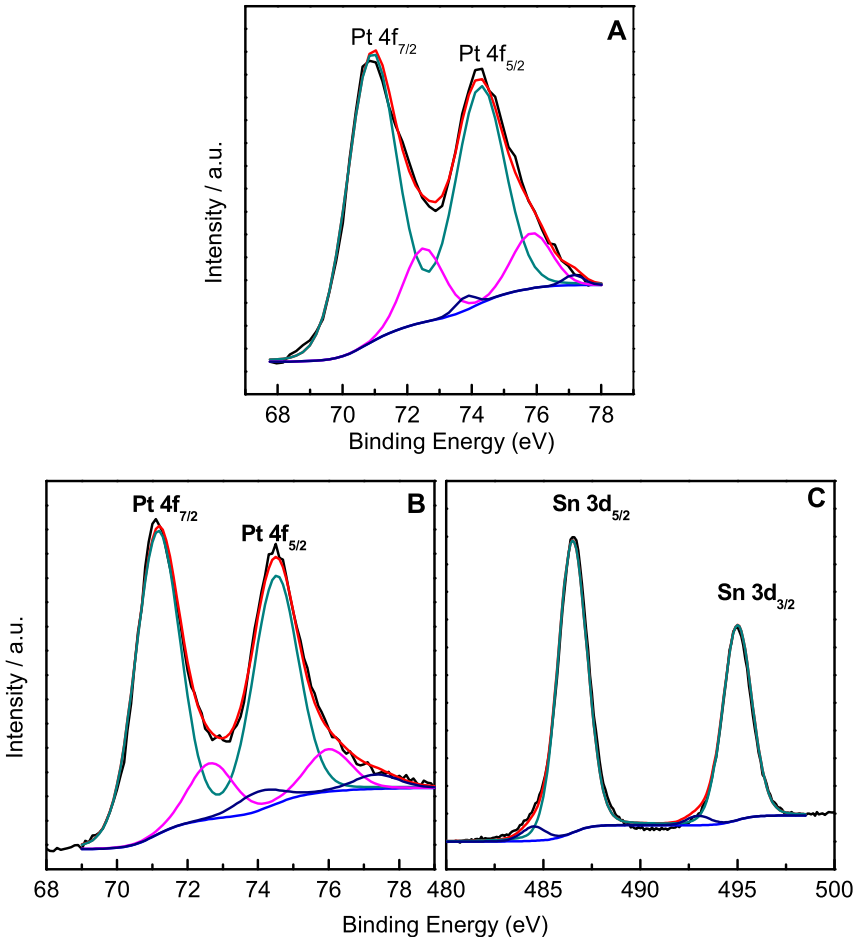

Fig. 3. Pt 4f XPS spectra for MPPt (A) and MPPt/Sn ($\theta_{Sn} = 0.60$) (B). Sn 3d XPS spectra for MPPt/Sn ($\theta_{Sn} = 0.60$) (C).

Table 1
XPS results for MPPt/Sn electrode.

Catalyst	$Pt_{species}$	Pt $4f_{7/2}$/eV (%at.)	$Sn_{species}$	Sn $3d_{5/2}$/eV)	Pt:Sn (%at.)	Pt:Sn (%wt.)
MPPt	Pt(0)	70.9 (67)	Sn(0)	–	–	–
	Pt(II)	71.9 (26)	Sn(IV)	–		
	Pt(IV)	73.1 (7)				
MPPt/Sn	Pt(0)	71.0 (80)	Sn(0)	484.4 (4)	40:60	51:49
($\theta_{Sn} = 0.60$)	Pt(II)	72.5 (14)	Sn(IV)	486.3 (96)		
	Pt(IV)	73.8 (5)				

currents, pointing out that the CO_{ad} oxidation reaction occurs in the 0.2–0.95 V_{RHE} potential range. Even more, due to the absence of interference associated to the double layer charging, oxide formation or other reaction different to CO_2 formation, the MSCV allows a better determination of the onset potential for the CO_{ad} oxidation reaction. In this context, the ionic current signal $m/z = 44$ rises at more negative potentials (a shift close to 0.06 V can be discerned) than that observed for the faradaic current. Moreover, by means of MSCV, the onset potential for the CO_2 production at MPPt/Sn electrode is detected at 0.2 V_{RHE}. The last value is lower than that observed by *in-situ* FTIRS utilized in a potentiostatic mode [45]. Furthermore, it is observed that the CO tolerance increases in the following way: MPPt << Pt_3Sn/C < MPPt/Sn. This order is not only confirmed by the onset potential for CO_{ad} oxidation reaction, but also by the increment of the $m/z = 44$ signal at more negative potentials. In other words, ionic current developed at 0.4 V is higher on MPPt/Sn than on Pt_3Sn/C material. In this context, Sn oxides deposited on mesoporous metallic Pt sites appear to be relevant for an enhanced activity towards the CO oxidation reaction.

On the other hand, a clear anodic peak (I) appears for the CO oxidation onto MPPt/Sn, which is absent for carbon supported PtSn, while the anodic contribution (II) occurs at more negative potentials for MPPt/Sn catalyst in comparison with the commercial catalyst. The first anodic peak (I) is related to high abundance of reactive sites. In this sense, low-coordinated Sn atoms, which can be presented as kink or step on the Pt surface, are reactive sites that may promote the formation of oxygenated species onto the surface (Sn–OH and SnO_2) at lower potentials than conventional PtSn alloys [45,46]. In this sense, it is well documented that CO stripping on Pt basal planes is more reactive on open than close-packed surfaces in acidic media [37], i.e. surface sites with (110) and (100) orientations are more reactive than that with (111) sites. Therefore, the higher CO tolerance can be associated to facile water dissociation on Pt open surfaces. As was discussed above and observed at Fig. 2, Sn adatoms as SnO_2 species (see XPS analysis at Table 1) are mainly deposited on MPPt sites with (110) and (100) orientations. Moreover, CO does not adsorb on Sn surfaces and consequently the formation of adsorbed oxygenated species (OH) is assured. The last does not occur on Ru-based materials (e.g. PtRu), in which CO_{ad} and water dissociation (OH_{ad} formation) compete for the same adsorption sites. For all the exposed reasons, the onset potential for CO stripping on MPPt/Sn is located at more negative potential when is compared with those experiments performed at

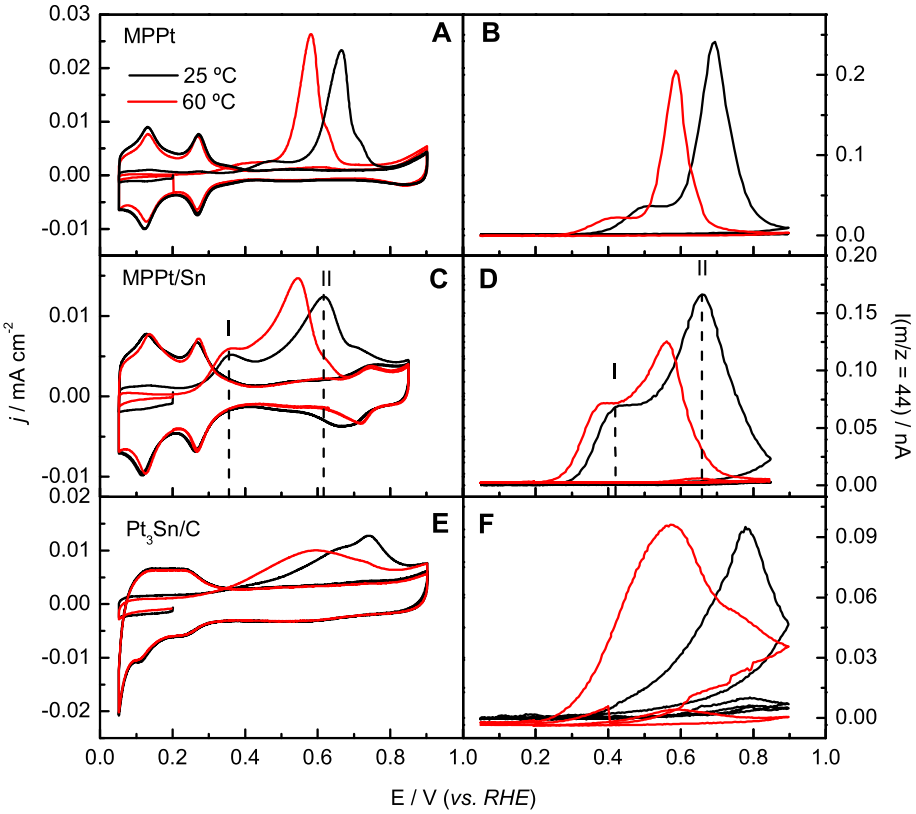

Fig. 4. CVs (left panels) and MSCVs (right panels) for CO_{ad} oxidation on MPPt (A, B); MPPt/Sn ($\theta_{Sn} = 0.60$) (C,D) and commercial Pt_3Sn/C (E, F) in 0.5 M H_2SO_4. Scan rate 5 mV s^{-1}; T = 25 and 60 °C.

MPPtRu, MPPt/Ru and PtRu/C materials [23,24].

3.3. Methanol oxidation on MPPt and MPPt/Sn ($\theta_{Sn} = 0.60$) catalysts

The potentiodynamic oxidation of methanol on MPPt (top panel), MPPt/Sn (middle panel) and Pt_3Sn/C E-TEK (bottom panel) recorded by cyclic voltammetry and DEMS can be seen in Fig. 5. Theoretical faradic currents calculated from the $m/z = 44$ signals after the calibration procedure were included (left panels, red lines). Note that the difference in area between experimental (black curve) and theoretical (red curve) faradaic currents is the extra charge associated with the formation of different products than CO_2 (e.g. formaldehyde and formic acid), and therefore, the CO_2 conversion efficiency can be estimated. Additionally, the ionic current related to methyl formate ($m/z = 60$) that is produced by the condensation reaction of methanol and formic acid, is depicted in the right panels of Fig. 5. Thus, formic acid production can be followed through this signal.

Interestingly, the onset potentials for faradaic current and formic acid formation are similar for both MPPt and MPPt/Sn. However, the peak potential for formic acid production (right panels) appears at more negative potentials than those observed for the faradaic current (black lines, left panels) at these electrodes. The last indicates that a by-side product such as formaldehyde is favored at high potentials at mesoporous electrodes. In this sense, it is difficult to distinguish between methanol and formaldehyde ionic signals, since both molecules develop the same m/z signals. On the other hand, the $m/z = 60$ signal for the carbon-supported material develops a completely different profile which can be explained assuming the slow diffusion of formic acid out of the porous structure of the carbon (this diffusion is favored in the mesoporous materials respect to the carbon supported ones as previously shown in Ref. [24]). The current efficiency to CO_2 (as average of the forward and backward scans) is higher for the MPPt (74%) than for the MPPt/Sn materials (46%). Indeed, the CO_2 conversion efficiency increases in the following way: MPPt/Sn < Pt_3Sn/C < MPPt (Table 2), although the experimental faradaic current density shows the opposite trend.

As stated above, the incomplete oxidation of methanol produces by-side reaction products, such as formaldehyde, formic acid and adsorbed reaction intermediates (mainly CO_{ad}). In fact, the decrease in the formation of these soluble side products produces a subsequent increase of the CO_2 conversion current efficiency, but this effect is not necessary accompanied by an increase in the recorded faradaic current density. Thus, the commercial Pt_3Sn/C catalyst develops lower faradaic current density than the MPPt/Sn electrode but higher CO_2 conversion efficiency. Therefore the lower current density can be associated to surface poisoning (blocking effect) by adsorbed species (e.g. adsorbed CO, formaldehyde or formic acid) that further oxidize to carbon dioxide, causing the rise of the energy conversion efficiency. In the same sense, thin catalytic MPPt/Sn films produce higher current densities and lower CO_2 formation than thick films (not shown), as faster diffusion is favored for the former avoiding further reaction of side products on the catalyst surface. Conversely, MPPt catalyst presents the highest CO_2 efficiency and also the most intense signal for formic acid. As will be shown later, this result can only be explained assuming a low production of formaldehyde at this electrode.

The influence of the morphology on the catalytic activity was confirmed comparing the results for the MPPt material with a Pt electrode prepared by electrodeposition following the same

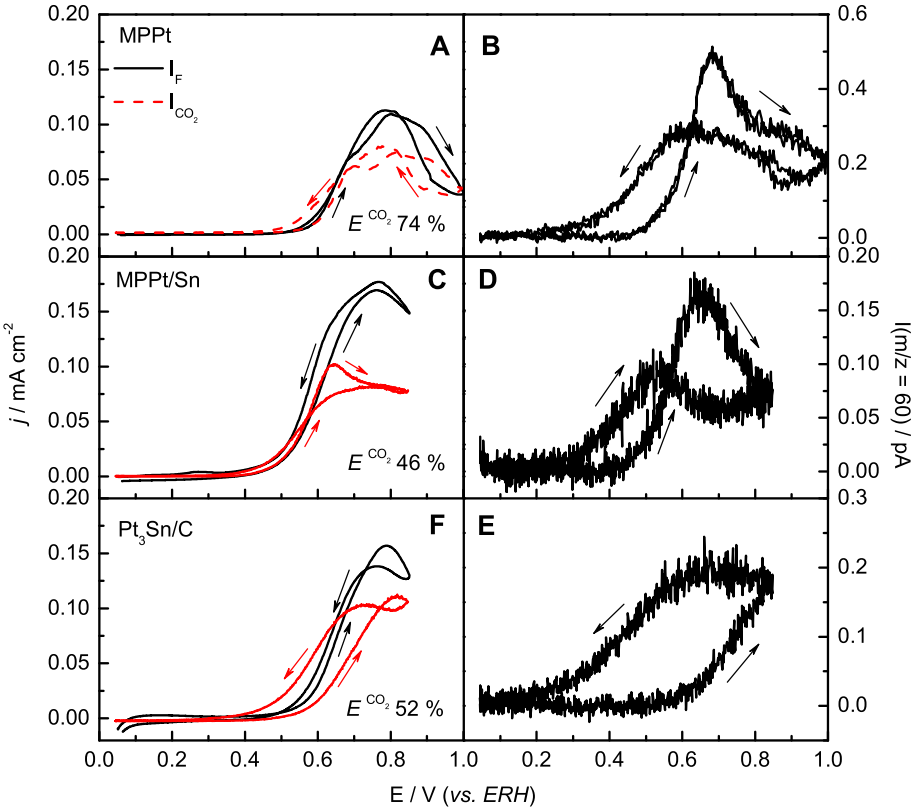

Fig. 5. CVs and MSCVs for methanol oxidation on MPPt (top panels), MPPt/Sn ($\theta_{Sn} = 0.60$) (middle panels) and Pt_3Sn/C (bottom panels) catalysts in 0.1 M CH_3OH + 0.5 M H_2SO_4 at 25 °C. Scan rate = 2 mV s^{-1}. Left panels: experimental (black line) and theoretical (from $m/z = 44$, red line) faradaic currents. Right panels: $HCOOCH_3$ ($m/z = 60$) formed by the condensation reaction of methanol and formic acid. (For interpretation of the references to color in this figure legend, the reader is referred to the web version of this article.)

Table 2
Efficiency conversion from methanol to CO_2 at 25 and 60 °C.

E(mV)	MPPt		MPPt/Sn		PtSn/C	
	Efficiency to CO_2 conversion					
	25 °C	60 °C	25 °C	60 °C	25 °C	60 °C
550[a]	95	100	100	84	96	73
650[a]	65	71	78	68	71	50
E_{total}	74	54	46	59	52	59

E_{total}: Efficiency conversion to CO_2 calculated from CVs.
[a] Efficiency conversion to CO_2 calculated from chronoamperometry.

procedure used for the MPPt but in the absence of surfactant. The cyclic voltammograms (see Supporting Information, Figs. 1S and 2S) show that higher current densities are obtained with the MPPt, concluding that higher activity can be achieved with the mesoporous structure. In concordance with results from Fig. 5 previously discussed, the lower current densities for the electrodeposited Pt are accompanied with a higher efficiency to CO_2 (80% for the electrodeposited Pt in the absence of surfactant and 74% for MPPt at 25 °C).

On the other hand, the chemical nature of the catalytic material appears as an important factor for both, the energy conversion efficiency and the current density. Left panels of Fig. 5 show that the onset potential for methanol oxidation on MPPt/Sn and MPPt electrodes is located at 0.4 and 0.5 V respectively. Both electrodes are smooth surfaces, in which reaction products diffuse in a similar way. However, Sn significantly improves the methanol oxidation reaction but not the CO_2 conversion efficiency at high potentials. Therefore, diverse pathways during the methanol oxidation reaction are operating at both mesoporous surfaces depending on the applied potentials. Actually, Sn deposition on Pt sites with (110) and (100) orientations enhances the CO tolerance and decreases the overpotential needed for the methanol oxidation reaction. Additionally, low production of formic acid is observed on Sn-containing electrodes. Consequently, the low CO_2 conversion efficiency and the high current delivered at E > 0.60 V for MPPt/Sn are associated to soluble formaldehyde formation.

Fig. 6 depicts the experimental (top panels) and theoretical (bottom panels) faradaic currents calculated from the CO_2 signal $m/z = 44$ and recorded at 0.55 and 0.65 V (25 °C). It is observed that the experimental faradaic current depends on the catalytic nature of the electrode and increases in the following way: Pt_3Sn/C < MPPt << MPPt/Sn, in good agreement with that observed in the potentiodynamic experiments (Fig. 5). Additionally, methanol conversion to CO_2 is almost complete for Pt–Sn catalysts at 0.55 V (Table 2), but decreases at 0.65 V, whereas the faradaic current increases. In this sense, Fig. 5 also displays a CO_2 conversion drop at potentials higher than 0.60 V. Opposite, for MPPt the current density increases with the applied potential and also does the current efficiency for CO_2 production. These results indicate, firstly, that the full methanol oxidation to CO_2 occurs not only through the adsorbed carbon monoxide path: MPPt increases the efficiency to CO_2 with the applied potential whereas decreases at Pt–Sn materials, being the former less tolerant to CO according to Fig. 4. In fact, the formic acid path, presumably by adsorbed formate, contributes also to carbon dioxide formation. The latter is in agreement with infrared results previously published [47–49]. Secondly, considering that formic acid also contributes to CO_2 formation, methanol conversion drop to CO_2 at Pt–Sn materials should be then associated to formaldehyde production instead of formic acid at 0.65 V.

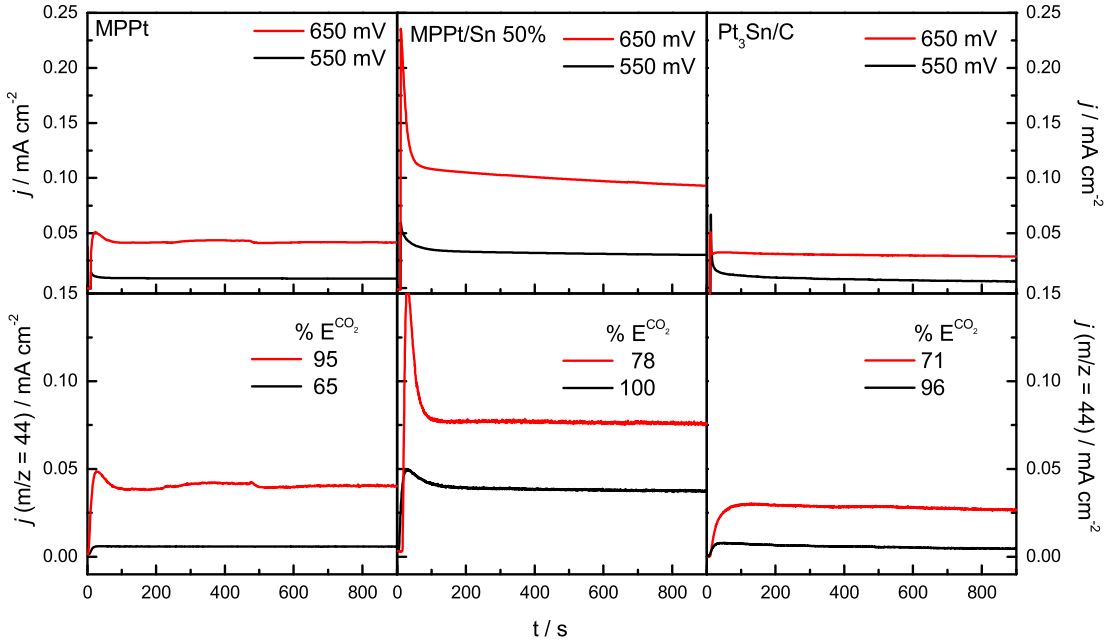

Fig. 6. Current transients for methanol electrooxidation at MPPt (left panels), MPPt/Sn ($\theta_{Sn} = 0.60$) (middle panels) and Pt_3Sn/C (right panels) at 0.55 (red line) and 0.65 V (black line) in 0.1 M CH_3OH + 0.5 M H_2SO_4 at 25 °C. Experimental (top panels) and theoretical (bottom panels) faradaic currents. (For interpretation of the references to color in this figure legend, the reader is referred to the web version of this article.)

The effect of the increment of the temperature up to 60 °C can be seen in Figs. 7 and 8. The curves in Fig. 7 show a raise of the current density for all catalysts with the temperature, being especially noticeable for MPPt/Sn. The onset potential for methanol oxidation at 60 °C remains with a similar trend to that observed at 25 °C, i.e. MPPt/Sn < Pt_3Sn/C < MPPt. Interestingly, the CO_2 conversion

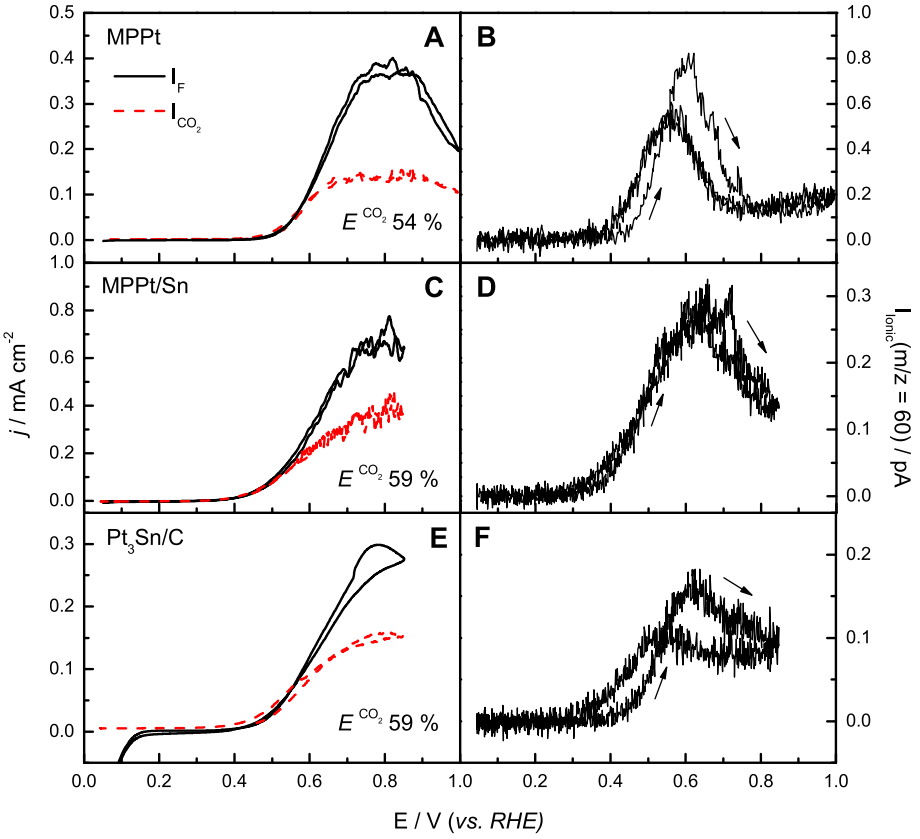

Fig. 7. CVs and MSCVs for methanol oxidation on MPPt (top panels), MPPt/Sn ($\theta_{Sn} = 0.60$) (middle panels) and Pt_3Sn/C (bottom panels) catalysts in 0.1 M CH_3OH + 0.5 M H_2SO_4 at 60 °C. Scan rate = 2 mV s^{-1}. Left panels: experimental (black solid line) and theoretical faradaic (red dash line) currents. Right panels: $HCOOCH_3$ ($m/z = 60$) formed by the condensation reaction of methanol and formic acid. (For interpretation of the references to color in this figure legend, the reader is referred to the web version of this article.)

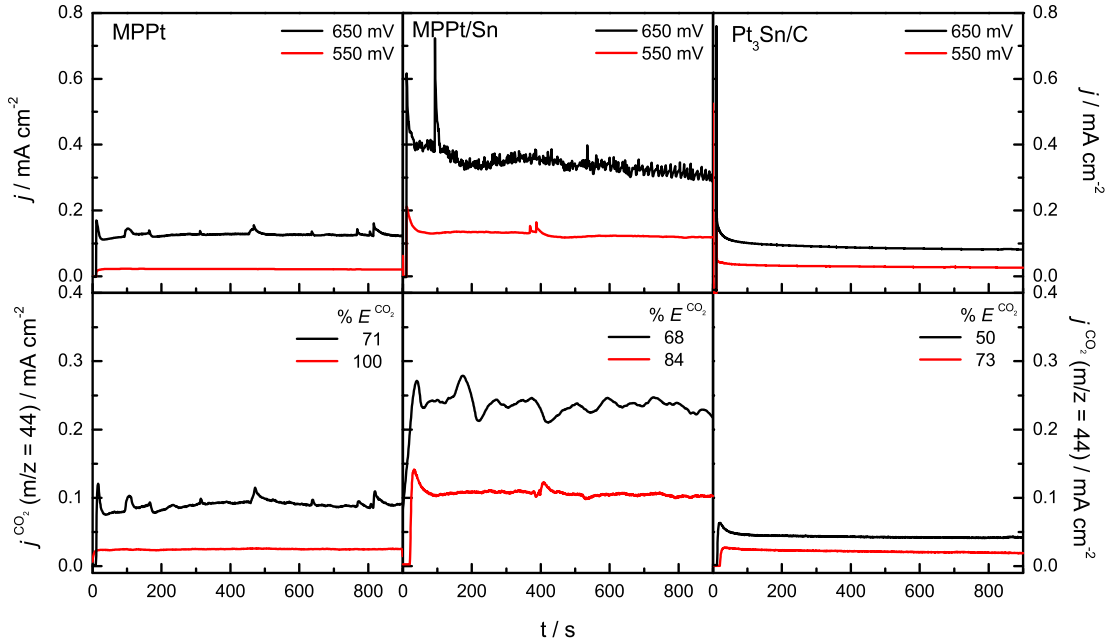

Fig. 8. Current transients for methanol electrooxidation at MPPt (left panels), MPPt/Sn ($\theta_{Sn} = 0.60$) (middle panels) and Pt_3Sn/C (right panels) at 0.55 (red line) and 0.65 V (black line) in 0.1 M CH_3OH + 0.5 M H_2SO_4 at 60 °C. Experimental (top panels) and theoretical (bottom panels) faradaic currents. (For interpretation of the references to color in this figure legend, the reader is referred to the web version of this article.)

efficiency diminishes for MPPt and growths for both electrodes containing Sn with the rise of the temperature (Table 2). Moreover, at 60 °C the intensity for the $m/z = 60$ signal increases notoriously, so the growth in the faradaic current is mainly related to the activation of the formic acid production pathway. It is observed that both ionic peak potentials for this signal (forward and backward scans) become similar in intensities and potential range, especially for the MPPt/Sn catalyst. This effect is explained by the enhancement of the water activation reaction with the rise of the temperature, increasing the kinetic and reversibility of the metallic oxide formation/reduction reaction.

Potentiostatic measurements at 0.55 and 0.65 V for methanol oxidation on all catalysts at 60 °C are depicted in Fig. 8. It can be established the following trend for recorded faradaic currents (upper panels): Pt_3Sn/C < MPPt << MPPt/Sn which also increase with the rise of the temperature, in concordance with the results in the CVs (Fig. 7). As explained before, the increment of the temperature facilitates the water dissociation onto metallic surfaces, and thereby, the CO tolerance. The higher CO_2 conversion occurs at 0.55 V, since the onset for formic acid production shifts to more negative potentials notoriously at 60 °C. Additionally, the presence of Sn onto the mesoporous electrode decreases the onset potential for the $m/z = 60$ signal associated to formic acid formation. Theoretical curves in Fig. 8 (bottom panels) show that at 60 °C the energy conversion efficiency from methanol to carbon dioxide at both applied potentials increases in the following way: Pt_3Sn/C < < MPPt/Sn ≤ MPPt. However, the highest delivered current by the MPPt/Sn suggests that this material presents the best performance toward methanol oxidation reaction. Indeed, it is expected for this catalyst high current density with elevated energy conversion efficiency at lower potentials (e.g. 0.45 V), in which low temperature fuel cells are operative.

Summarizing, the rise of the temperature promotes the water dissociation on metallic surfaces, thus producing an enhancement of both the CO and methanol oxidation reactions. The kinetic of methanol deprotonation process increases with the temperature and the applied potential, and then the formic acid formation is favored, although the current efficiency to CO_2 decreases. Adsorbed CO oxidation reaction is also favored with the temperature by the increment of the water activation process, and it is expected to liberate the surface for a fast methanol replacement. In this context, Sn does not adsorb CO but increases the rate of carbon monoxide removal, appearing as a better promoter than Ru for Pt-based materials. All these parameters (high activity and conversion efficiency to CO_2) suggest a good performance toward methanol oxidation on Pt–Sn based materials at high temperatures and low overpotentials. In this context, Sn atoms adsorbed onto Pt open structures (MPPt/Sn) present higher tolerance than Pt–Sn alloys toward CO.

On the other hand, product (carbon dioxide, formaldehyde and formic acid) diffusion away from the active site is fast on well-structured mesoporous surfaces, and consequently, the turnover rate of methanol at these surfaces is high. Thus, mesoporous electrodes exhibit high faradaic currents during the methanol oxidation reaction; meanwhile the introduction of Sn improves the conversion efficiency to CO_2 [50]. Thus, commercial Pt_3Sn/C catalyst develops elevated conversion efficiency but small current density, which is associated with a low turnover rate of methanol inside the carbon support structure.

4. Conclusions

Methanol oxidation on mesoporous Pt (MPPt) and Sn modified MPPt (MPPt/Sn) with 60% of Sn coverage ($\theta_{Sn} = 0.60$) was studied and compared with commercial carbon supported Pt_3Sn alloy at 25 and 60 °C in acidic media. Reaction intermediates and energy conversion efficiency from methanol to CO_2 were also investigated using a new configuration of the cell differential electrochemical mass spectrometry (DEMS). This setup allowed the use of a conventional electrochemical cell and a meniscus configuration can be adopted [29].

The presence of Sn onto the MPPt surface enhances the CO and methanol electrooxidation at low overpotentials due to the presence of Sn oxophilic atoms situated on an open surface structure. Sn

promotes the water dissociation but does not adsorb CO, and therefore the turnover rate of the fuel is accurate. Consequently, the bifunctional mechanism appears to be operative, i.e. oxygenated tin species are able to supply oxygenated species (OH) at lower potentials than Pt, resulting in an enhancement of CO and methanol electrooxidation reactions.

The rate of the electrocatalytic process increases with the temperature and the applied potential. Thus, best performance is obtained with MPPt/Sn catalyst at low potentials and high temperatures. High potentials produce high faradaic currents due to formation of side products mainly as formaldehyde, with the subsequent decrease of the conversion efficiency to CO_2.

Mesoporous structures appear as suitable electrodes to replace carbon supported material in low temperature fuel cells. This appreciation arises from carbon corrosion that produces catalyst dissolution and agglomeration, and consequently loss of fuel cell performance. However, mesoporous materials are stable and possess high electronic conductivity in acidic media. Moreover, the porous structure facilitates the diffusion of soluble products away of the catalysts site, increasing in this way the turnover rate and consequently allowing catalyst active sites reutilization.

Acknowledgments

The authors gratefully acknowledge financial support given by the Spanish MINECO under the project CTQ2011-28913-C02-02 and PRI-AIRBAR-2011-1307 for the cooperation between both groups. P.S.C acknowledges CONICET (Argentine) for the doctoral fellowship. J.F-M. is indebted to the ACIICI (Gobierno de Canarias) for the predoctoral fellowship. G.A. Planes is a permanent research fellow of CONICET.

Appendix A. Supplementary data

Supplementary data related to this article can be found at http://dx.doi.org/10.1016/j.jpowsour.2015.02.018.

References

[1] C. Lamy, A. Lima, V. LeRhun, F. Dlime, C. Coutanceau, J.M. Leger, Recent advances in the development of direct alcohol fuel cells (DAFC), J. Power Sources 105 (2002) 283–296.
[2] R. O'Hayre, S.W. Cha, W. Collela, F.B. Prinz, Fuel Cells Fundamentals, Second ed., Wiley, Hoboken, NJ, 2009.
[3] J. Larminie, A. Dicks, Fuel Cells Systems Explained, Wiley, Hoboken, NJ, 2003.
[4] G. Hoogers, Fuel Cell Technology Handbook, CRC Press, Boca Raton, FL, 2003.
[5] M. Watanabe, S. Motoo, Electrocatalysis by ad-atoms: part II. Enhancement of the oxidation of methanol on platinum by ruthenium ad-atoms, J. Electroanal. Chem. 60 (1975) 267–273.
[6] M. Watanabe, Y. Genjima, K. Turumi, Direct methanol oxidation on platinum electrodes with ruthenium adatoms in hot phosphoric acid, J. Electrochem. Soc. 144 (1997) 423–428.
[7] K.L. Ley, R. Liu, C. Pu, Q. Fan, N. Leyarovska, C. Segre, E.S. Smotkin, Methanol oxidation on single-phase Pt-Ru-Os ternary alloys, J. Electrochem. Soc. 144 (1997) 1543–1548.
[8] M. Götz, H. Wendt, Binary and ternary anode catalyst formulations including the elements W, Sn and Mo for PEMFCs operated on methanol or reformate gas, Electrochim. Acta 43 (1998) 3637–3644.
[9] M. Lefèvre, J.P. Dodelet, Fe-based catalysts for the reduction of oxygen in polymer electrolyte membrane fuel cell conditions: determination of the amount of peroxide released during electroreduction and its influence on the stability of the catalysts, Electrochim. Acta 48 (2003) 2749–2760.
[10] R.W. Reeve, P.A. Christensen, A. Hamnett, S.A. Haydock, S.C. Roy, Methanol tolerant oxygen reduction catalysts based on transition metal sulfides, J. Electrochem. Soc. 145 (1998) 3463–3471.
[11] T.J. Schmidt, U.A. Paulus, H.A. Gasteiger, N. Alonso-Vante, R.J. Behm, Oxygen reduction on $Ru_{1.92}Mo_{0.08}SeO_4$, Ru/carbon, and Pt/carbon in pure and methanol-containing electrolytes, J. Electrochem. Soc. 147 (2000) 2620–2624.
[12] B. Beden, L. Lamy, A. Bewick, K. Kunimatsu, Electrosorption of methanol on a platinum electrode. IR spectroscopic evidence for adsorbed CO species, J. Electroanal. Chem. 121 (1981) 343–347.
[13] S. Sakka, Handbook of Sol-Gel Science and Technology, Kluwer AP, Dordrecht, 2004.
[14] P.K. Jal, S. Patel, B.K. Mishr, Chemical modification of silica surface by immobilization of functional groups for extractive concentration of metal ions, Talanta 62 (2004) 1005–1028.
[15] T.S. Zhao, C. Xu, R. Chen, W.W. Yang, Mass transport phenomena in direct methanol fuel cells, Prog. Energy Combust. Sci. 35 (2009) 275–292.
[16] Y. Tokudome, K. Nakanishi, K. Kanamori, K. Fujita, H. Akamatsu, T. Hanada, Structural characterization of hierarchically porous alumina aerogel and xerogel monoliths, J. Colloid Interface Sci. 338 (2009) 506–513.
[17] W.H. Lizcano-Valbuena, V.A. Paganin, C.A.P. Leite, F. Galembeck, E.R. Gonzalez, Catalysts for DMFC: relation between morphology and electrochemical performance, Electrochim. Acta 48 (2003) 3869–3878.
[18] W.H. Lizcano-Valbuena, D.C. Azevedo, E.R. Gonzalez, Supported metal nanoparticles as electrocatalysts for low-temperature fuel cells, Electrochim. Acta 49 (2004) 1289–1295.
[19] E. Antolini, J.R.C. Salgado, L.G.R.A. Santos, G. Garcia, E.A. Ticcianelli, E. Pastor, E.R. Gonzalez, Carbon supported Pt-Cr alloys as oxygen-reduction catalysts for direct methanol fuel cells, J. Appl. Electrochem. 36 (2006) 355–362.
[20] H. Liu, C. Song, L. Zhang, J. Zhang, H. Wang, D.P. Wilkinson, A review of anode catalysis in the direct methanol fuel cell, J. Power Sources 155 (2006) 95–110.
[21] E. Antolini, Formation of carbon-supported PtM alloys for low temperature fuel cells: a review, Mater. Chem. Phys. 78 (2003) 563–573.
[22] J. Jiang, A. Kucernak, Electrooxidation of small organic molecules on mesoporous precious metal catalysts: II: CO and methanol on platinum–ruthenium alloy, J. Electroanal. Chem. 543 (2003) 187–199.
[23] G.A. Planes, G. García, E. Pastor, High performance mesoporous Pt electrode for methanol electrooxidation. A DEMS study, Electrochem. Commun. 9 (2007) 839–844.
[24] G. García, J. Florez-Montaño, A. Hernandez-Creus, E. Pastor, G.A. Planes, Methanol electrooxidation at mesoporous Pt and Pt–Ru electrodes: a comparative study with carbon supported materials, J. Power Sources 196 (2011) 2979–2986.
[25] A. Kucernak, J. Jiang, Mesoporous platinum as a catalyst for oxygen electroreduction and methanol electrooxidation, Chem. Eng. J. 93 (2003) 81–90.
[26] T.F. Esterle, A.E. Russell, P.N. Bartlett, Study of carbon monoxide oxidation on mesoporous platinum, ChemPhysChem. 11 (2010) 2896–2905.
[27] A. Crown, C. Johnston, A. Wieckowski, Growth of ruthenium islands on Pt (*hkl*) electrodes obtained via repetitive spontaneous deposition, Surf. Sci. 506 (2002) L268–L274.
[28] J.S. Spendelow, P.K. Babu, A. Wieckowski, Electrocatalytic oxidation of carbon monoxide and methanol on platinum surfaces decorated with ruthenium, Curr. Opin. Solid State Mater. Sci. 9 (2005) 37–48.
[29] S. Pérez-Rodríguez, M. Corengia, G. García, C.F. Zinola, M.J. Lázaro, E. Pastor, Gas diffusion electrodes for methanol electrooxidation studied by a new DEMS configuration: influence of the diffusion layer, Int. J. Hydrog. Energy 37 (2012) 7141–7151.
[30] E. Lamy-Pitara, J. Barvier, Platinum modified by electrochemical deposition of adatoms, Appl. Catal. A 149 (1997) 49–87.
[31] H. Massong, S. Tillmann, T. Langkau, E.A. Abd El Meguid, H. Baltruschat, On the influence of tin and bismuth UPD on Pt(111) and Pt(332) on the oxidation of CO, Electrochim. Acta 44 (1998) 1379–1388.
[32] H. Massong, H. Wang, G. Samjeské, H. Baltruschat, The co-catalytic effect of Sn, Ru and Mo decorating steps of Pt (111) vicinal electrode surfaces on the oxidation of CO, Electrochim. Acta 46 (2001) 701–707.
[33] X.Y. Xiao, S. Tillmann, H. Baltruschat, Scanning tunneling microscopy of Sn coadsorbed with Cu and CO on Pt (111) electrodes, Phys. Chem. Chem. Phys. 4 (2002) 4044–4050.
[34] A.A. El-Shafei, M. Eiswirth, Electrochemical activity of Sn-modified Pt single crystal electrodes for ethanol oxidation, Surf. Sci. 604 (2010) 862–867.
[35] S.S. Gupta, S. Singh, J. Datta, Temperature effect on the electrode kinetics of ethanol electro-oxidation on Sn modified Pt catalyst through voltammetry and impedance spectroscopy, Mater. Chem. Phys. 120 (2010) 682–690.
[36] E. Antolini, E.R. Gonzalez, Effect of synthesis method and structural characteristics of Pt–Sn fuel cell catalysts on the electro-oxidation of CH_3OH and CH_3CH_2OH in acid medium, Catal. Today 160 (2011) 28–38.
[37] G. García, M.T.M. Koper, Carbon monoxide oxidation on Pt single crystal electrodes: understanding the catalysis for low temperature fuel cells, ChemPhysChem. 12 (2011) 2064–2072.
[38] S. Stalnionis, L. Tamasauskaite-Tamasiunaite, V. Pautieniene, A. Sudavicius, Z. jusys, Modification of a Pt surface by spontaneous Sn deposition for electrocatalytic applications, J. Solid State Electrochem. 8 (2004) 892–899.
[39] J.F. Moulder, W.F. Stickle, P.E. Sobol, K.D. Bomben, Jill Chastain (Eds.), Handbook of X-ray Photoelectronic Spectroscopy, Perkin-Elmer Corp, Eden Prairie, MN, USA, 1992.
[40] D. Teschner, A. Wootsch, Z. Paál, Preferential CO oxidation in hydrogen (PROX) on unsupported PtSn catalyst, Appl. Catal. A 411–412 (2012) 31–34.
[41] M. Arenz, K.J.J. Mayrhofer, V. Stamenkovic, B.B. Blizanac, T. Tomoyuki, P.N. Ross, N.M. Markovic, The effect of the particle size on the kinetics of CO electrooxidation on high surface area Pt catalysts, J. Am. Chem. Soc. 127 (2005) 6819–6829.
[42] E. Antolini, E.R. González, The electro-oxidation of carbon monoxide, hydrogen/carbon monoxide and methanol in acid medium on Pt-Sn catalysts for low-temperature fuel cells: a comparative review of the effect of Pt-Sn structural characteristics, Electrochim. Acta 56 (2010) 1–14.
[43] D.M. Dos Anjos, F. Hahn, J.M. Léger, K.B. Kokoh, G. Tremiliosi-Filho, Ethanol electrooxidation on Pt-Sn and Pt-Sn-W bulk alloys, J. Braz. Chem. Soc. 19

(2008) 795–799.
[44] O. Guillen-Villafuerte, G. García, R. Guil-Lopez, E. Nieto, J.L. Rodriguez, G. Fierro, E. Pastor, Carbon monoxide and methanol oxidations on Pt/X@ MoO_3/C (X = Mo_2C, MoO_2, Mo^0) electrodes at different temperatures, J. Power Sources 231 (2013) 163–172.
[45] M. Arenz, V. Stamenkovic, B.B. Blizanac, K.J. Mayrhofer, N.M. Markovic, P.N. Ross, Carbon-supported Pt–Sn electrocatalysts for the anodic oxidation of H_2, CO, and H_2/CO mixtures: part II: the structure–activity relationship, J. Catal. 232 (2005) 402–410.
[46] V. Del Colle, J. Souza-García, G. Tremiliosi-Filho, E. Herrero, J.M. Feliu, Electrochemical and spectroscopic studies of ethanol oxidation on Pt stepped surfaces modified by tin adatoms, Phys. Chem. Chem. Phys. 13 (2011) 12163–12172.
[47] A. Cuesta, M. Escudero, B. Lanova, H. Baltruschat, Cyclic voltammetry, ftirs, and dems study of the electrooxidation of carbon monoxide, formic acid, and methanol on cyanide-modified Pt (111) electrodes, Langmuir 25 (2009) 6500–6507.
[48] M. Osawa, K. Komatsu, G. Samjeské, T. Uchida, T. Ikeshoji, A. Cuesta, C. Gutierrez, The role of bridge-bonded adsorbed formate in the electrocatalytic oxidation of formic acid on platinum, Angew. Chem. Int. 50 (2011) 1159–1163.
[49] A. Cuesta, G. Cabello, M. Osawa, C. Gutierrez, Mechanism of the electrocatalytic oxidation of formic acid on metals, ACS Catal. 2 (2012) 728–738.
[50] Y. Ishikawa, M. Sheng Liao, C.R. Cabrera, Oxidation of methanol on platinum, ruthenium and mixed Pt–M metals (M = Ru, Sn): a theoretical study, Surf. Sci. 463 (2000) 66–80.